7-14-2017

Spin-polarized two-dimensional electron gas at GdTiO3/SrTiO3 interfaces: Insight from first-principles calculations

J. Betancourt
University of Puerto Rico, San Juan

Tula R. Paudel
University of Nebraska-Lincoln, tula.paudel@gmail.com

Evgeny Y. Tsymbal
University of Nebraska at Lincoln, tsymbal@unl.edu

J. P. Velev
University of Puerto Rico, San Juan, jvelev@gmail.com

Spin-polarized two-dimensional electron gas at $GdTiO_3/SrTiO_3$ interfaces: Insight from first-principles calculations

J. Betancourt,[1] T. R. Paudel,[2] E. Y. Tsymbal,[2] and J. P. Velev[1,2,*]

[1]*Department of Physics and Astronomy, University of Puerto Rico, San Juan, Puerto Rico 00931, USA*

[2]*Department of Physics and Astronomy, University of Nebraska, Lincoln, Nebraska 68588, USA*

(Received 30 January 2017; revised manuscript received 8 May 2017; published 14 July 2017)

Two-dimensional electron gases (2DEGs) at oxide interfaces have been a topic of intensive research due to their high carrier mobility and strong confinement. Additionally, strong correlations in the oxide materials can give rise to new and interesting physics, such as magnetism and metal-insulator transitions at the interface. Using first-principles calculations based on density functional theory, we demonstrate the presence of a highly spin-polarized 2DEG at the interface between the Mott insulator $GdTiO_3$ and a band insulator $SrTiO_3$. The strong correlations in the dopant cause ferromagnetic alignment of the interface Ti atoms and result in a fully spin-polarized 2DEG. The 2DEG consists of two types of carriers distinguished by their orbital character. The majority of the interface charge is strongly localized on the Ti d_{xy} orbitals at the interface and a smaller fraction resides on the delocalized Ti $d_{xz,yz}$ states.

DOI: 10.1103/PhysRevB.96.045113

I. INTRODUCTION

The ability to grow atomically abrupt oxide interfaces has enabled the new field of oxide electronics [1–4]. A key development is the discovery of a two-dimensional electron gas (2DEG) at the interfaces between two insulators $SrTiO_3$ and $LaMO_3$ (M = Ti, Al, or V) [5–9]. One of the advantages of oxide 2DEGs, over the semiconducting analogs, is that oxide materials exhibit a wide variety of properties, such as magnetism and ferroelectricity. These properties can be utilized as means to engineer new functionalities. Examples include interfaces with ferroelectric oxides, where the ferroelectric polarization is used to control the 2DEG charge density [10–12] and interfaces with ferromagnetic oxides, where the magnetization of the host induces spin polarization of the 2DEG [13,14].

The mechanism of the 2DEG formation in the $LaMO_3/SrTiO_3$ (001) and similar systems is attributed to a polar discontinuity at the interface. Along the [001] direction, the $LaMO_3$ consists of alternating $(LaO)^{+1}$ and $(MO_2)^{-1}$ charged planes, whereas the $SrTiO_3$ consists of alternating $(SrO)^0$ and $(TiO_2)^0$ neutral planes. Thus, when $LaMO_3$ is grown on the TiO_2-terminated surface of $SrTiO_3$, the polar discontinuity at the interface creates an increasing electric potential in the system. To eliminate the diverging potential, ½ electron is transferred from the surface of $LaMO_3$ to the $LaMO_3/SrTiO_3$ interface, a mechanism which is known as electronic reconstruction induced by polar catastrophe [15]. A charge transfer to the interface may also occur in the $LaMO_3/SrTiO_3$ (001) superlattices if the $LaMO_3$ layer is nonstoichiometric and terminated with the LaO monolayers on both sides [in a limiting case, a monolayer of LaO replaces a monolayer of SrO in a $SrTiO_3$ (001) crystal]. In this case, an "extra" electron is introduced into the system due to the uncompensated ionic charge on the additional $(LaO)^{+1}$ monolayer, a mechanism which is equivalent to electron doping [16]. The origin and confinement of the 2DEG at $LaMO_3/SrTiO_3$ interfaces has been the subject of numerous first-principles studies, which largely confirm these mechanisms [17–26]. The formation of the 2DEG has also been observed in other oxide systems, such as wurtzite ZnO/Zn(Mg)O interfaces, where the different polarization in the two materials leads to polarization discontinuity at the interface [27,28].

Standard electronic devices, such as field effect transistors, make use of the charge of the carriers to process information. Using the spin of the electrons to carry information is advantageous, not only because of the improved energy efficiency, but also because it enables new device paradigms such as spin transistors [29]. Therefore, spin-polarized 2DEG is of particular interest for spintronics applications. It has been shown that magnetism can be induced at the interface between the nonmagnetic insulators $LaAlO_3/SrTiO_3$ [30–32]. However, the magnetism appears to be weak, Stoner-type exchange splitting produced by geometric confinement of the carriers in the $SrTiO_3$ slab [33,34]. A number of other systems have been predicted theoretically to support spin-polarized 2DEGs, including Stoner-type magnetism in $LaAlO_3/FeS_2$ [35], and systems with magnetic insulators to host the 2DEG such as in $LaMnO_3/SrMnO_3$ [13] or $LaAlO_3/EuO$ [14,36].

Recently, rare-earth titanates, other than $LaTiO_3$, have also been used to interface with $SrTiO_3$. These materials are known to be affected by strong electron-electron correlations that can be used to engineer interfacial metallic or charge-ordered states. For example, doping of $SrTiO_3$ lattices with a single layer of rare-earth oxide can result in either conducting (La, Pr, Nd) or charge-ordered (Sm, Y) state depending on the dopant [37]. A great deal of work has been reported on $GdTiO_3/SrTiO_3$ interfaces, at which a very high-charge density 2DEG has been observed in a variety of geometries, such as $GdTiO_3$ doped with single layers of SrO [38,39], $SrTiO_3$ quantum wells embedded in $GdTiO_3$ [40], $GdTiO_3/SrTiO_3$ superlattices [41,42], and single interfaces [43,44].

As a consequence of the strong electronic correlations, the rare-earth titanates reveal interesting magnetic properties [45–47]. The compounds containing rare-earth atoms with larger ionic radius, such as $LaTiO_3$, exhibit a G-type

*jvelev@gmail.com

antiferromagnetic order where Ti atoms are antiferromagnetically ordered in the pseudocubic (001) plane [45]. However, with decreasing ionic radius, there is a transition to ferromagnetic ordering of the Ti atoms in the (001) plane [45,46]. In particular, $GdTiO_3$ has a ferrimagnetic ground state, where the Ti $3d$ moments are aligned in the (001) plane and antiferromagnetically aligned to the Gd $4f$ moments in the neighboring planes [46]. Furthermore, $GdTiO_3$ doping has been shown experimentally to induce spin polarization of the 2DEG at low temperatures: magnetization and hysteresis of the magnetoresistance have been observed in both $SrTiO_3$ quantum wells embedded in $GdTiO_3$ [48–50] and thin $GdTiO_3$ layers embedded in $SrTiO_3$ host [51,52].

First-principles calculations based on density functional theory (DFT) have yielded a great deal of insight in the physics of oxide interfaces. In the case of rare-earth titanates, such first-principles calculations have been employed in a variety of ways. On the most fundamental level, the bulk band structure of the titanates was used to infer the band alignment at interfaces between titanates and other perovskite oxides [53,54]. A major area of research has been the study of metal-insulator transition induced by single-layer doping of strongly correlated oxides. Supercell calculations have been performed on single layers of rare-earth oxides (La,Y) [37] embedded in $SrTiO_3$ host and conversely single layers of SrO doping of $GdTiO_3$ [55]. Bulk calculations show that the metal-insulator transition in $SrTiO_3$ embedded $GdTiO_3$ can be explained by the high charge density doping due to the interface charge [56]. Another important area of research, where first-principles calculations have been applied, is the effect of the boundary conditions on the critical thickness for the appearance of the 2DEG and the charge density of the 2DEG at these interfaces. Such calculations have been carried out for band insulator/band insulator interfaces ($LaAlO_3/SrTiO_3$) and band insulator/Mott insulator interfaces ($GdTiO_3/SrTiO_3$) [57,58]. Finally, *ab initio* band structure has been used to interpret angle-resolved photoemission (ARPES) measurements of the 2DEG at the interface of small-period $GdTiO_3/SrTiO_3$ superlattices [42].

In this paper, we use first-principles DFT calculations to investigate the formation, distribution, and properties of 2DEG at the interface between the band insulator $SrTiO_3$ and the Mott insulator $GdTiO_3$. By making the parallel to the 2DEG at the $LaTiO_3/SrTiO_3$ (001) interface, we show that the stronger electron-electron correlations at the $GdTiO_3/SrTiO_3$ (001) interface lead to the ferromagnetic alignment of the Ti magnetic moments and a fully spin-polarized 2DEG. We find that the 2DEG consists of two types of carriers, distinguished by their orbital character and characterized by different spatial distribution and mobility.

II. METHODS AND STRUCTURE

In the study of the electronic structure of $RTiO_3/SrTiO_3$ (R = La,Gd) heterostructures, we use first-principles DFT calculations within the projected augmented wave approach as implemented in the Vienna *Ab initio* Simulation Package (VASP) [59]. The exchange-correlation effects are treated within the Perdew-Burke-Ernzerhof (PBE) generalized gradient approximation for the density functional [60]. The rare-earth titanates are Mott insulators with one electron in the Ti $3d$ band. This necessitated the use of Hubbard U to account for strong electron correlations (PBE + U) [61]. We use the Hubbard parameters $U = 8.5$ eV for R $4f$ and $U = 3.0$ eV for Ti $3d$ electrons previously reported in the literature [37,55]. The self-consistent calculations are performed using a plane-wave basis set limited by a cutoff energy of 500 eV, $8 \times 8 \times 1$ Monkhorst-Pack k-point mesh in the Brillouin zone, and energy convergence threshold of 10^{-6} eV/cell. For the self-consistent and density of states (DOS) calculations, Methfessel-Paxton smearing was used with smearing width 0.05 eV. The standard VASP PBE pseudopotentials were used. Both La and Gd have the valence configuration $5s6s5p5d4f$ with occupation of 11 and 18 electrons, respectively.

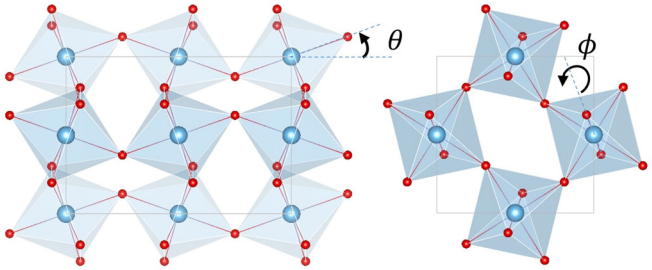

FIG. 1. Side and top view of $RTiO_3$ in the $GaFeO_3$ crystal structure. The octahedral tilts (θ) and rotations (ϕ) are indicated. The rare earth atoms, in between the octahedral, are not shown for clarity.

Before we proceed with the study of the heterostructures, we calculate the electronic structure of bulk $RTiO_3$. The rare-earth titanates grow in the $GaFeO_3$ crystal structure [47], shown in Fig. 1, which derives from the cubic perovskite structure ($Pm\bar{3}m$) with rotations and tilts of the Ti octahedra around the c axis, lowering the symmetry to orthorhombic ($Pbnm$). The octahedral rotations are the same for each plane but opposite within the plane, while the octahedral tilts are opposite on all neighboring octahedra. As a result, the unit cell size increases to $\sqrt{2} \times \sqrt{2} \times 2$ with two Ti atoms in the (001) plane. In our case, the in-plane lattice constant a is fixed to the calculated value for cubic $SrTiO_3$ (3.95 Å). The c axis lattice constant and the ionic coordinates are optimized while retaining the orthorhombic symmetry of the crystal. The atomic structure optimization is performed within PBE + U until the Hellmann-Feynman forces on each atom become less than 1.0 meV/Å.

We compare two titanates, $LaTiO_3$ and $GdTiO_3$, which differ by the occupation of the f orbitals and the atomic radius of the rare-earth atom [46]. The structural optimization of bulk $GdTiO_3$ grown on $SrTiO_3$ substrate gives a c/a ratio of 1.431. The magnitudes of the octahedral tilts and rotations are $\theta = 19.4^\circ$ and $\phi = 12.8^\circ$, respectively. Bulk $LaTiO_3$ grows in the same $GaFeO_3$ crystal structure as $GdTiO_3$. However, due to the larger ionic radius of La, the c/a ratio is larger, 1.490, and the octahedral tilts and rotations are smaller, $\theta = 16.5^\circ$ and $\phi = 11.7^\circ$, than those in $GdTiO_3$.

The band structure of bulk $GdTiO_3$ and the corresponding DOS are shown in Fig. 2. The band structure indicates that the material is a Mott insulator with a band gap of about

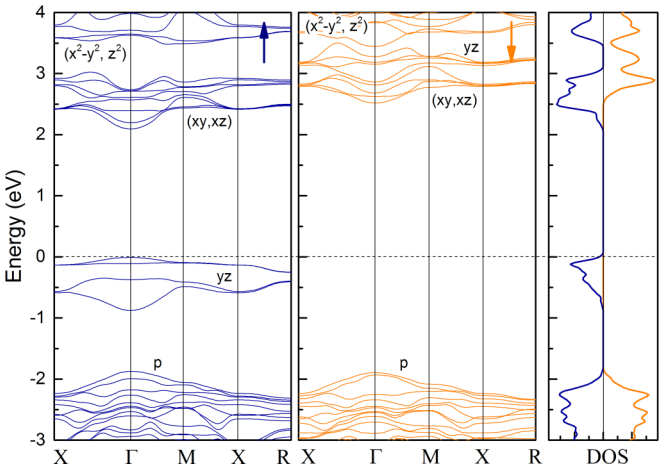

FIG. 2. Spin-polarized band structure (left panels) and corresponding DOS (right panel) of bulk $GdTiO_3$. Majority- (blue curves) and minority- (orange curves) spin contributions are indicated by up- and down-pointing arrows, respectively. The Fermi level is at zero energy. The orbital character of the bands is indicated.

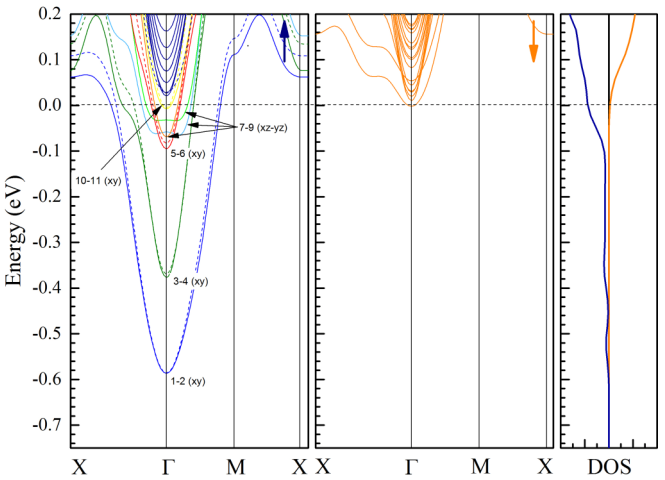

FIG. 3. Band structure and DOS of $(GdTiO_3)_1/(SrTiO_3)_{13}$ superlattice around the Fermi level. The partially occupied bands are color-coded and numbered. Their orbital character is indicated in the brackets.

2 eV, which opens due to the lifting of the degeneracy of the Ti t_{2g} majority states. The magnetic ground state of $GdTiO_3$ is ferrimagnetic, where the Ti magnetic moments of $1.0\mu_B$ are ferromagnetically coupled in the (001) plane and antiferromagnetically coupled to the Gd magnetic moments of $7.0\mu_B$ in the neighboring planes. These properties are different from $LaTiO_3$ (see the Supplemental Material [62]). Although electronically $LaTiO_3$ is also a Mott insulator, the magnetic ordering in $LaTiO_3$ is G-type antiferromagnetic, with the Ti magnetic moments of 1.0 μ_B antiferromagnetically aligned to their neighbors. Due to the antiferromagnetic order, the band structure of $LaTiO_3$ is spin independent (see the Supplemental Material [62]), although it is locally different for majority- and minority-spin states.

The magnetic ordering of the rare-earth titanates is determined by a competition between the antiferromagnetic R-O-Ti and Ti-O-Ti interactions [46]. The main driver of these interactions is the difference in the rare-earth atom's f orbital configuration. In addition, the smaller atomic radius in the heavier rare-earths is associated with smaller lattice volume and stronger R-O-Ti interaction. In the case of $LaTiO_3$, the La atoms have no magnetic moment; thus, the R-O-Ti interaction does not play a role. As the result, the Ti-O-Ti superexchange interaction leads to a G-type antiferromagnetic ordering of the Ti atoms in the plane. In the case of later rare-earth titanates, the R-O-Ti interaction is mediated by the partial overlap between the unoccupied R $4f$ orbitals and the Ti $3d$ orbitals. In Gd, the $4f$ orbitals are half filled. The occupied majority f band resides between 8–9 eV below the Fermi level, and its main role is to produce the magnetic moment on the Gd atom. The unoccupied f band resides between 5–6 eV above the Fermi level and is hybridized with the unoccupied Ti $3d$ band. This hybridization is responsible for breaking the spin degeneracy of the Ti t_{2g} band, resulting in the magnetic moment on the Ti atom. In $GdTiO_3$, the Gd-O-Ti coupling dominates, causing both the Gd and Ti atoms to order ferromagnetically in the plane and antiferromagnetically with each other [46].

III. RESULTS AND DISCUSSION

With this preliminary information, we turn to the study of $RTiO_3/SrTiO_3$ (R = La,Gd) heterostructures. In order to obtain the distribution of the 2DEG in the depth of the $SrTiO_3$ host, we consider fairly large superlattices consisting of $\sqrt{2} \times \sqrt{2} \times 14$ unit cells. Within these, up to three SrO layers are replaced with RO, and the corresponding octahedral distortions are introduced as in the bulk structures. The atomic positions within the supercell are then optimized. In both cases, the octahedral distortions of the rare-earth titanate cause similar distortions in the neighboring layers of the $SrTiO_3$ host. Generally, the optimized structures show that the octahedral rotations die out in the $SrTiO_3$ host very quickly; however, octahedral tilts decrease more gradually (see the Supplemental Material [62]). The octahedral tilts approach zero within 6–7 unit cells from the interface, while the octahedral rotations vanish within three unit cells.

We first consider the case of doping of the $SrTiO_3$ (001) slab with a single layer of RO [37]. The resulting atomic structure is equivalent to R atoms substituting Sr atoms in the SrO monolayer of $SrTiO_3$. The electronic structure of the $(GdTiO_3)_1/(SrTiO_3)_{13}$ superlattice around the Fermi level is shown in Fig. 3. Due to the mirror symmetry of the structure, the bands come in nearly degenerate pairs, one for each equivalent Ti atom on either side of the interface. We have assumed the convention that each pair of bands is drawn in a different color, and one of the bands is indicated with a solid line and the other with a dashed line. The breaking of the degeneracy is due to the interaction of the bands through the GdO layer. The band structure in a larger energy scale is given in the Supplemental Material [62].

The principal observation following from Fig. 3 is that the interface is nearly half metallic. It is seen that there are partially occupied majority-spin Ti $3d$ states, while the minority-spin Ti $3d$ band is nearly empty. This is due to balance between the total electron charge at the interface and the exchange splitting of the spin bands, which places the Fermi energy at

the bottom of the minority-spin band. The total amount of charge is one electron per Gd atom, when Gd^{3+} ion substitutes Sr^{2+} in the SrO monolayer of $SrTiO_3$. This charge is equally shared between Ti atoms in $SrTiO_3$ above and below the GdO layer, resulting in ½ electron charge per "interface."

The electron correlations induce significant distortions of the Ti octahedra around the GdO layer (see the Supplemental Material [62]); however, they are smaller than the distortions in the bulk $GdTiO_3$ and not sufficient to lift the degeneracy of the Ti t_{2g} levels and cause a Mott transition. This results in the interface-induced charge residing in the partially filled t_{2g} band on the Ti atoms close to the interface. Similar results are obtained in the case of the $(LaTiO_3)_1/(SrTiO_3)_{13}$ superlattice (see the Supplemental Material [62]). In that case also, the electronic correlations are not strong enough to lift the degeneracy of the Ti t_{2g}, and the 2DEG resides in the partially occupied t_{2g} band [37]. However, in the case of LaO doping, the 2DEG is not spin polarized.

As for the bulk materials, this difference between $LaTiO_3$ and $GdTiO_3$ interfaces can be explained by the f orbital occupation of the rare-earth atoms and the strength of the R-O-Ti interaction. In the case of LaO doping, the La f orbitals are unoccupied, and the R-O-Ti interaction does not play a role. In this case, the Ti atoms at the interface order independently and antiferromagnetically, and the induced interface charge is distributed equally between the minority- and majority-spin channels. On the contrary, the half-filled f band of Gd and its small atomic radius result in strong coupling between the Gd and the Ti atoms. Therefore, the Ti atoms at the interface order ferromagnetically in the plane, and the induced interface charge resides in only one spin band. The charge is confined at the interface by the electrostatic potential, which is established in the process of electronic and ionic screening.

The DOS at the Fermi level is evidence for the presence of nearly 100% spin-polarized 2DEG. We can obtain further details of the 2DEG distribution by projecting the bands on particular atoms and orbitals. The obtained spatial distribution of the 2DEG in the depth of the $SrTiO_3$ host is shown in Fig. 4. This charge density is obtained from integration of the orbital-decomposed charge density in the energy window of the 2DEG, i.e. between $E = -0.6$ eV (bottom of the 2DEG) and the Fermi level in Figs. 3. The numbering and color-coding of the bands corresponds to that in Fig. 3. Bands of different color correspond to atoms positioned at a different distance from the interface. From the total charge density of the 2DEG, we can see that the 2DEG is strongly localized close to the interface, and the charge density decreases in the bulk of the host. Figures 3 and 4 provide evidence for two types of confinement resulting from orbital ordering. The majority of the charge is strongly localized on the in-plane d_{xy} orbitals of particular Ti planes. There are four pairs of nearly degenerate d_{xy} bands (1–6,10–11 in Fig. 3), one from each interface, crossing the Fermi level which are localized on the four Ti layers closest to the interface. More than 90% of the total 2DEG charge resides on these levels, of which more than 60% is localized on the interface Ti atoms. In addition to this in-plane localized charge, less than 10% of the charge is delocalized throughout the slab. This charge resides in three out-of-plane bands with d_{xz} and d_{yz} characters (7–9 on Fig. 3).

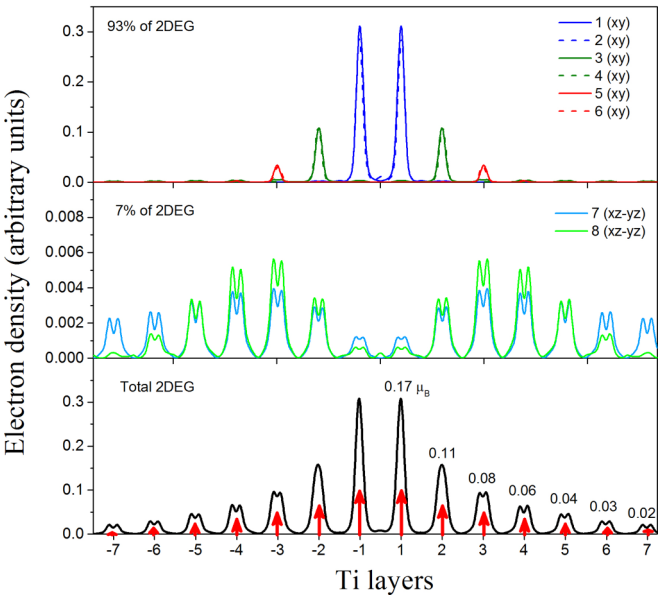

FIG. 4. Space and band decomposition of the 2DEG charge density in the $(GdTiO_3)_1/(SrTiO_3)_{13}$ superlattice. Bottom panel shows the total 2DEG charge density. The top two panels show the charge density of the individual bands crossing the Fermi level, grouped by orbital character. The numbers and coloring correspond to Fig. 3. The x axis numbers are the Ti layers on either side of the interface. The arrows in the bottom panel represent the magnetic moment per Ti atom.

Instead of talking about spin-degenerate and spin-polarized 2DEG, in the case of LaO and GdO doping, respectively, we can interpret the results in terms of induced magnetization at the interface. In the case of LaO doping, the net magnetization induced at the interface is zero, while GdO doping induces magnetic moments on the Ti atoms close to the interface. The size of the magnetic moments per Ti on each layer is indicated in Fig. 4, and the total magnetic moment is $0.5\mu_B$ per Ti per interface.

The existence of two types of carriers in the 2DEG has been shown in calculations of $LaXO_3/SrTiO_3$(X = Al,Ti) interfaces [21,22,63], and evidence of the $d_{xz,yz}$ character of the 2DEG far from the interface has been observed experimentally [64]. This orbital ordering, which affects the 2DEG distribution and properties, is a direct consequence of the nontrivial band structure of the $SrTiO_3$ host. This separation of the 2DEG into a strongly confined portion, conducting strictly in-plane, and a more dispersed portion could have potentially interesting consequences. One implication is that the strictly 2D part of the 2DEG can be localized by defects and not participate in the transport, which could partially explain the discrepancy between theoretical predications and experimental observations of the amount of interface charge [21]. Another option is that, by controlling the electrostatic boundary conditions, less than the nominal 0.5 electron per interface can be introduced to the interface [57,58]. Thus, it could be achieved that all the charge resides at a single layer at the interface, resulting in an artificial strictly 2D system.

Single-layer doping of the host lattice is a very special case of $RTiO_3/SrTiO_3$ (001) superlattices, where there is no

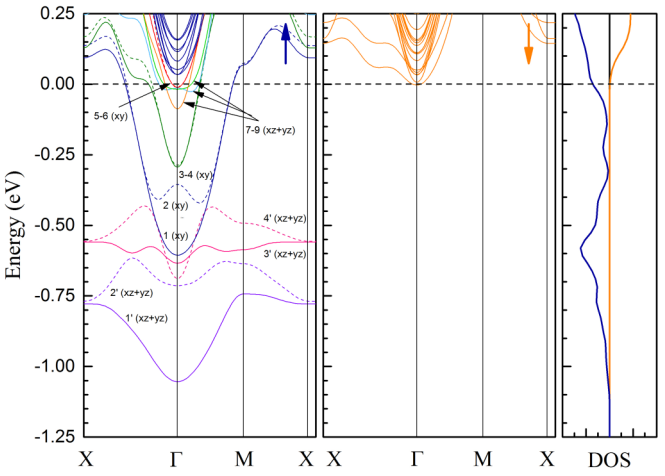

FIG. 5. Band structure and DOS of $(GdTiO_3)_3/(SrTiO_3)_{11}$ superlattice around the Fermi level. The partially occupied bands are color-coded and numbered. Their orbital character is indicated in the brackets.

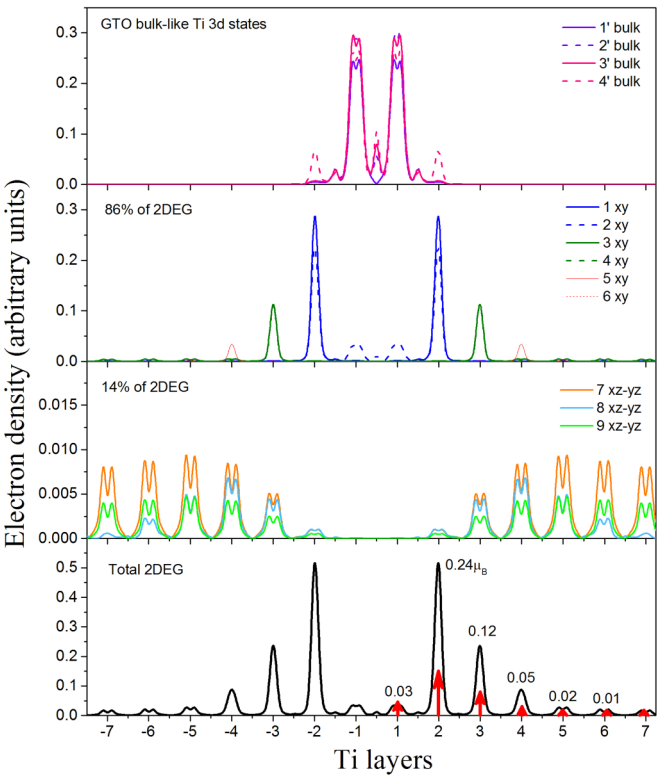

FIG. 6. Space and band decomposition of the 2DEG charge density in the $(GdTiO_3)_3/(SrTiO_3)_{11}$ superlattice. Bottom panel shows the total 2DEG charge density. The top three panels the charge density of the individual bands crossing the Fermi level. The numbers and coloring correspond to Fig. 5. The arrows in the bottom panel represent the magnetic moment per Ti atom.

proper bulk rare-earth titanate. Thus, the next step in this paper is to increase the size of the RTiO$_3$ doped region. We consider $(RTiO_3)_3/(SrTiO_3)_{11}$ superlattices, which is the thinnest RTiO$_3$ slab to have at least one RO layer not at the interface. The electronic structure of the GdTiO$_3$/SrTiO$_3$ superlattice is shown in Fig. 5 around the Fermi level and in the Supplemental Material in a larger energy scale [62]. Similar to the previous case, the total amount of charge is 1/2 electron per Ti atom per interface due to RO doping. We find that the interface is still half metallic. However, in the bulk of the GdTiO$_3$ slab, the electron correlations become strong enough to induce a Mott transition. In the GdTiO$_3$ slab, the t_{2g} levels of the Ti atoms split, producing the occupied bands located between -0.5 and -1.0 eV below the Fermi level. These bands reside on the Ti atoms below the interface and do not participate in the transport. On the contrary, in the Ti atoms at the interface and in the bulk of the host, the degeneracy is still present, and the carriers occupy partially filled Ti t_{2g} bands. The first pair of 2DEG bands (1–2 in Fig. 5) overlaps in energy and hybridizes strongly with the bulk Ti bands (1′–4′), which breaks their degeneracy. The bands further away from the interface are not affected and are very similar to those in the single-layer doping case (Fig. 3). These results corroborate recent theoretical calculations of small-period GdTiO$_3$/SrTiO$_3$ heterostructures aiming to correlate the electronic structure at the interface to the results of ARPES measurements [42]. The results of Ref. [42] also predict a nearly fully spin-polarized 2DEG and a different spatial dependence of the orbitals with the d_{xy} and $d_{xz,yz}$ character. They fail, however, to capture the decay length of the 2DEG into the bulk SrTiO$_3$ due to the small thickness of the SrTiO$_3$ layer used in their calculations.

We obtain similar results for the electronic structure of $(LaTiO_3)_3/(SrTiO_3)_{11}$ superlattices (see the Supplemental Material [62]). Here, the Mott transition in the bulk of the LaTiO$_3$ slab also takes place, producing the occupied band around -1.0 eV. In this case, the octahedral distortions are smaller, and there is less charge transfer between the Ti and O atoms, which results in smaller band dispersion of this state. The t_{2g} levels on the interface and the host Ti atoms are still degenerate, forming the partially occupied band where the 2DEG resides. As before, the Ti moments are antiferromagnetically aligned, and the band structure is the same for the majority- and minority-spin channels. The charge is equally distributed between the spin channels. The smaller occupation of each spin channel, together with the smaller band dispersion of the bulk Ti bands, causes the bulk Ti and the 2DEG bands not to overlap in energy as in the case of $(GdTiO_3)_3/(SrTiO_3)_{11}$ superlattices.

The spatial distribution of the 2DEG charge density for the $(GdTiO_3)_3/(SrTiO_3)_{11}$ superlattice is shown in Fig. 6. The lowest lying bands (1′–4′) reside on the Ti atoms in the bulk of the GdTiO$_3$ slab. The partially occupied bands (1–9) reside on the Ti atoms at the interface and in the host. As before, there are two types of confinement. The majority of the charge is strongly localized on the d_{xy} orbitals of the three Ti planes closest to the interface (1–6). Due to the hybridization between the bulk and interface Ti bands in the majority-spin channel, some of the 2DEG penetrates in the bulk of the GdTiO$_3$ slab, which is evident from the satellite peaks in the top panel of Fig. 6. A smaller portion of the charge, residing on out-of-plane d_{xz} and d_{yz} orbitals, is delocalized in the host.

In order to obtain further insight in the confinement of the 2DEG, we plot in Fig. 7 the unit cell averaged charge density for both $(GdTiO_3)_1/(SrTiO_3)_{13}$ and $(GdTiO_3)_3/(SrTiO_3)_{13}$

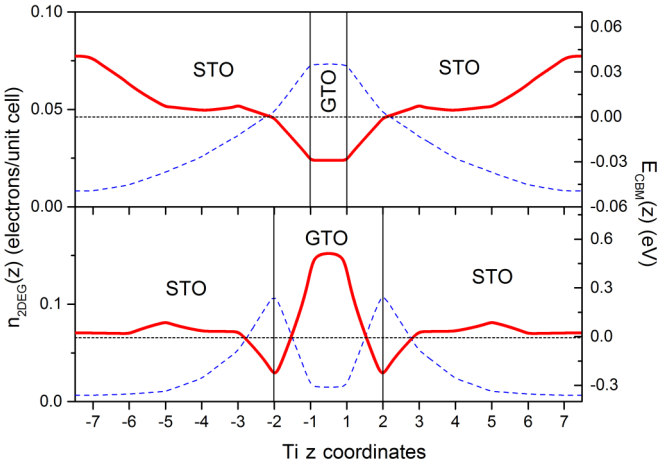

FIG. 7. Macroscopically averaged 2DEG charge density (blue dashed line) and the corresponding confining potential (red solid line) for (a) $(GdTiO_3)_1/(SrTiO_3)_{13}$ and (b) $(GdTiO_3)_3/(SrTiO_3)_{11}$ superlattices.

superlattices. We obtain the charge density of the 2DEG, n_{2DEG}, for the energy window below the Fermi energy containing the 2DEG, while manually removing bound states coming from Ti atoms in the interior of the $GdTiO_3$ slab in the latter case. Close to the interface the dielectric constant ε varies with position. Therefore, the Poisson equation has the form $\varepsilon V'' + \varepsilon' V' = n_{2DEG}$, and solving it requires knowledge of the spatial variation of the dielectric constant close to the interface.

Instead of doing that, we solve the one-dimensional Schrodinger equation $-\frac{1}{m^*}\psi'' + V\psi = E\psi$ with the constraint $|\psi|^2 = n_{2DEG}$, where the effective mass m^* is obtained from the band dispersion of the 2DEG bands close to the Γ point, and it is assumed to be constant. Thus, ψ is an effective wave function having the property that it reproduces the charge density of the 2DEG. Inverting this equation at the Fermi level ($E = 0$), we obtain the effective confining potential V that the electrons in the 2DEG experience. In the case of doping with a single layer, Fig. 7 (top panel), the confining potential is a shallow potential well which is consistent with the metallicity of the GdO layer. The LaO doping case is qualitatively similar and differs only by the depth of the potential well (see the Supplemental Material [62]). These results support the conclusion that the embedding of a single layer of RO in $SrTiO_3$ host suppresses the Mott transition in the rare-earth titanate. The potential plot shows that the classical electrostatic potential extends over the interface Ti atoms. The charge on those is electrostatically confined. From there, the charge tunnels into the $SrTiO_3$ host, which accounts for the exponential decay of the 2DEG charge density. The plot of the 2DEG charge density is not quite a straight line in logarithmic scale. Instead, it appears to be a superposition of a couple of different decay rates, one large and one significantly smaller. This is consistent with the spatial distribution of the charge shown in Figs. 4 and 6. The large rate of decay corresponds to the localized charge on the d_{xy} orbitals and the smaller rate of decay to the charge on the $d_{xz,yz}$ orbitals. The stronger hybridization between the out-of-plane orbitals on different layers contributes to the latter.

In the case of $(GdTiO_3)_3/(SrTiO_3)_{11}$ (Fig. 7, bottom panel), there is a barrier in the $GdTiO_3$ slab which is due to the fact that the material undergoes a Mott transition in the bulk and the slab becomes insulating. The confining potential in the case of a $LaTiO_3$ slab is the same except for the height of the barrier (see the Supplemental Material [62]). These results demonstrate that one bulk TiO_2 layer is sufficient to induce the Mott transition. The classical confining potential extends over the interface Ti layers from where the charge tunnels into the bulk of the host. Again, the plot of the 2DEG charge density indicates multiple rates of decay.

IV. CONCLUSIONS

Overall, our calculations show that interfaces between the ferrimagnetic Mott insulator $GdTiO_3$ and the band insulator $SrTiO_3$ supports a half-metallic 2DEG. The 2DEG exhibits large charge density of 1/2 electron per interface. The spin polarization of the 2DEG is due to the strong electronic correlations in the $GdTiO_3$, which cause the Ti moments at the interface to be aligned ferromagnetically in the plane. We also find that, in the case of doping of the host with a single RO layer, the Mott transition is suppressed, making the doping layer metallic, while in doping with a thicker $RTiO_3$ layer, the Mott transition in the bulk of the doping layer makes it insulating. Finally, we also find that nontrivial orbital ordering in the $SrTiO_3$ host results in two types of carriers with different confinement and mobilities. The first carrier type is strongly confined at the interface, and it is localized at particular Ti planes. The second type resides on out-of-plane orbitals, which are dispersed and penetrate deeper in the host.

ACKNOWLEDGMENTS

This paper was supported by the National Science Foundation (Grants No. EPS-1002410, No. EPS-1010094, and No. DMR-1105474). Computations were performed at the Holland Computing Center at the University of Nebraska–Lincoln.

[1] J. Mannhart and D. G. Schlom, Oxide interfaces—An opportunity for electronics, Science **327**, 1607 (2010).
[2] P. Zubko, S. Gariglio, M. Gabay, P. Ghosez, and J.-M. Triscone, Interface physics in complex oxide heterostructures, Ann. Rev. Cond. Matt. Phys. **2**, 141 (2011).
[3] J. Chakhalian, A. J. Millis, and J. Rondinelli, The interface is still the device, Nat. Mater. **11**, 92 (2012).
[4] H. Y. Hwang, Y. Iwasa, M. Kawasaki, B. Keimer, N. Nagaosa, and Y. Tokura, Emergent phenomena at oxide interfaces, Nat. Mater. **11**, 103 (2012).
[5] A. Ohtomo, D. A. Muller, J. L. Grazul, and H. Y. Hwang, Artificial charge-modulation in atomic-scale perovskite titanate superlattices, Nature **419**, 378 (2002).
[6] A. Ohtomo and H.Y. Hwang, A high-mobility electron gas at the $LaAlO_3/SrTiO_3$ heterointerface, Nature **427**, 423 (2004).

[7] S. Thiel, G. Hammerl, A. Schmehl, C. W. Schneider, and J. Mannhart, Tunable quasi-two-dimensional electron gases in oxide heterostructures, Science **313**, 1942 (2006).

[8] Y. Hotta, T. Susaki, and H. Y. Hwang, Polar Discontinuity Doping of the $LaVO_3/SrTiO_3$ Interface, Phys. Rev. Lett. **99**, 236805 (2007).

[9] M. Huijben, A. Brinkman, G. Koster, G. Rijnders, H. Hilgenkamp, and D. H. A. Blank, Structure-property relation of $SrTiO_3/LaAlO_3$ interfaces, Adv. Mater. **21**, 1665 (2009).

[10] M. K. Niranjan, Y. Wang, S. S. Jaswal, and E. Y. Tsymbal, Prediction of a Switchable Two-Dimensional Electron Gas at Ferroelectric Oxide Interfaces, Phys. Rev. Lett. **103**, 016804 (2009).

[11] M. S. J. Marshall, A. Malashevich, A. S. Disa, M.-G. Han, H. Chen, Y. Zhu, S. Ismail-Beigi, F. J. Walker, and C. H. Ahn, Conduction at a Ferroelectric Interface, Phys. Rev. Appl. **2**, 051001 (2014).

[12] P. Aguado-Puente, N. C. Bristowe, B. Yin, R. Shirasawa, Philippe Ghosez, P. B. Littlewood, and E. Artacho, Model of Two-Dimensional Electron Gas Formation at Ferroelectric Interfaces, Phys. Rev. B **92**, 035438 (2015).

[13] B. R. K. Nanda and S. Satpathy, Spin-Polarized Two-Dimensional Electron Gas at Oxide Interfaces, Phys. Rev. Lett. **101**, 127201 (2008).

[14] Y. Wang, M. K. Niranjan, J. D. Burton, J. M. An, K. D. Belashchenko, and E. Y. Tsymbal, Prediction of a spin-polarized two-dimensional electron gas at the $LaAlO_3$/EuO (001) interface, Phys. Rev. B **79**, 212408 (2009).

[15] N. Nakagawa, H. Y. Hwang, and D. A. Muller, Why some interfaces cannot be sharp?Nat. Mater. **5**, 204 (2006).

[16] N. C. Bristowe, P. Ghosez, P. B. Littlewood, and E. Artacho, The origin of two-dimensional electron gases at oxide interfaces: Insights from theory, J. Phys.: Condens. Matter **26**, 143201 (2014).

[17] Z. P. Popovic and S. Satpathy, Wedge-Shaped Potential and Airy-Function Electron Localization in Oxide Superlattices, Phys. Rev. Lett. **94**, 176805 (2005).

[18] M. S. Park, S. H. Rhim, and A. J. Freeman, Charge compensation and mixed valency in $LaAlO_3/SrTiO_3$ heterointerfaces studied by the FLAPW method, Phys. Rev. B **74**, 205416 (2006).

[19] S. Okamoto, A. J. Millis, and N. A. Spaldin, Lattice Relaxation in Oxide Heterostructures: $LaTiO_3/SrTiO_3$ Superlattices, Phys. Rev. Lett. **97**, 056802 (2006).

[20] J. Lee and A. A. Demkov, Charge origin and localization at the n-type $SrTiO_3/LaAlO_3$ interface, Phys. Rev. B **78**, 193104 (2008).

[21] Z. S. Popovic, S. Satpathy, and R. M. Martin, Origin of the Two-Dimensional Electron Gas Carrier Density at the $LaAlO_3$ on $SrTiO_3$ Interface, Phys. Rev. Lett. **101**, 256801 (2008).

[22] P. Larson, Z. S. Popović, and S. Satpathy, Lattice relaxation effects on the interface electron states in the perovskite oxide heterostructures: $LaTiO_3$ monolayer embedded in $SrTiO_3$, Phys. Rev. B **77**, 245122 (2008).

[23] R. Pentcheva and W. E. Pickett, Avoiding the Polarization Catastrophe in $LaAlO_3$ Overlayers on $SrTiO_3$ (001) Through Polar Distortion, Phys. Rev. Lett. **102**, 107602 (2009).

[24] K. Janicka, J. P. Velev, and E. Y. Tsymbal, Quantum Nature of Two-Dimensional Electron Gas Confinement at $LaAlO_3/SrTiO_3$ Interfaces, Phys. Rev. Lett. **102**, 106803 (2009).

[25] H. Chen, A. Kolpak, and S. Ismail-Beigi, First-principles study of electronic reconstructions of $LaAlO_3/SrTiO_3$ heterointerfaces and their variants, Phys. Rev. B **82**, 085430 (2010).

[26] H. Chen, A. M. Kolpak, and S. Ismail-Beigi, Electronic and magnetic properties of $SrTiO_3/LaAlO_3$ interfaces from first principles, Adv. Mater. **22**, 2881 (2010).

[27] A. Tsukazaki, A. Ohtomo, T. Kita, Y. Ohno, H. Ohno, and M. Kawasaki, Quantum Hall effect in polar oxide heterostructures, Science **315**, 1388 (2007).

[28] J. Betancourt, J. J. Saavedra-Arias, J. D. Burton, Y. Ishikawa, E. Y. Tsymbal, and J. Velev, Polarization discontinuity induced two-dimensional electron gas at ZnO/Zn(Mg)O interfaces: A first-principles study, Phys. Rev. B **88**, 085418 (2013).

[29] S. Datta and B. Das, Electronic analog of the electro-optic modulator, Appl. Phys. Lett. **56**, 665 (1990).

[30] A. Brinkman, M. Huijben, M. Van Zalk, J. Huijben, U. Zeitler, J. C. Maan, W. G. Van Der Wiel, G. Rijnders, D. H. A. Blank, and H. Hilgenkamp, Magnetic effects at the interface between non-magnetic oxides, Nat. Mater. **6**, 493 (2007).

[31] J.-S. Lee, Y.W. Xie, H. K. Sato, C. Bell, Y. Hikita, H. Y. Hwang, and C.-C. Kao, Titanium d_{xy} ferromagnetism at the $LaAlO_3/SrTiO_3$ interface, Nat. Mater. **12**, 703 (2013).

[32] F. Bi, M. Huang, S. Ryu, H. Lee, C.-W. Bark, C.-B. Eom, P. Irvin, and J. Levy, Room-temperature electronically-controlled ferromagnetism at the $LaAlO_3/SrTiO_3$ interface, Nat. Commun. **5**, 5019 (2014).

[33] K. Janicka, J. P. Velev, and E. Y. Tsymbal, Magnetism of $LaAlO_3/SrTiO_3$ superlattices, J. Appl. Phys. **103**, 07B508 (2008).

[34] N. Pavlenko, T. Kopp, E. Y. Tsymbal, J. Mannhart, and G. A. Sawatzky, Oxygen vacancies at titanate interfaces: Two-dimensional magnetism and orbital reconstruction, Phys. Rev. B **86**, 064431 (2012).

[35] J. D. Burton and E. Y. Tsymbal, Highly Spin-Polarized Conducting State at the Interface Between Nonmagnetic Band Insulators: $LaAlO_3/FeS_2$ (001), Phys. Rev. Lett. **107**, 166601 (2011).

[36] J. Lee, N. Sai, and A. A. Demkov, Spin-polarized two-dimensional electron gas through electrostatic doping in $LaAlO_3$/EuO heterostructures, Phys. Rev. B **82**, 235305 (2010).

[37] H. W. Jang, D. A. Felker, C. W. Bark, Y. Wang, M. K. Niranjan, C. T. Nelson, Y. Zhang, D. Su, C. M. Folkman, S. H. Baek, S. Lee, K. Janicka, Y. Zhu, X. Q. Pan, D. D. Fong, E. Y. Tsymbal, M. S. Rzchowski, and C. B. Eom, Metallic and insulating oxide interfaces controlled by electronic correlations, Science **331**, 886 (2011).

[38] D. G. Ouellette, P. Moetakef, T. A. Cain, J. Y. Zhang, S. Stemmer, D. Emin, and S. J. Allen, High-density two-dimensional small polaron gas in a delta-doped Mott insulator, Sci. Rep. **3**, 3284 (2013).

[39] P. Moetakef, C. A. Jackson, J. Hwang, L. Balents, S. J. Allen, and S. Stemmer, Toward an artificial Mott insulator: Correlations in confined high-density electron liquids in $SrTiO_3$, Phys. Rev. B **86**, 201102 (2012).

[40] J. Y. Zhang, C. A. Jackson, R. Chen, S. Raghavan, P. Moetakef, L. Balents, and S. Stemmer, Correlation between metal-insulator transitions and structural distortions in high-electron-density $SrTiO_3$ quantum wells, Phys. Rev. B **89**, 075140 (2014).

[41] P. Moetakef, T. A. Cain, D. G. Ouellette, J. Y. Zhang, D. O. Klenov, A. Janotti, C. G. Van de Walle, S. Rajan, S. J. Allen,

and S. Stemmer, Electrostatic carrier doping of $GdTiO_3/SrTiO_3$ interfaces, Appl. Phys. Lett. **99**, 232116 (2011).

[42] S. Nemsak, G. Conti, A. X. Gray, G. K. Palsson, C. Conlon, D. Eiteneer, A. Keqi, A. Rattanachata, A. Y. Saw, A. Bostwick, L. Moreschini, E. Rotenberg, V. N. Strocov, M. Kobayashi, T. Schmitt, W. Stolte, S. Ueda, K. Kobayashi, A. Gloskovskii, and W. Drube *et al.*, Energetic, spatial, and momentum character of the electronic structure at a buried interface: The two-dimensional electron gas between two metal oxides, Phys. Rev. B **93**, 245103 (2016).

[43] M. Boucherit, O. F. Shoron, T. A. Cain, C. A. Jackson, S. Stemmer, and S. Rajan, Extreme charge density $SrTiO_3/GdTiO_3$ heterostructure field effect transistors, Appl. Phys. Lett. **102**, 242909 (2013).

[44] M. Boucherit, O. Shoron, C. A. Jackson, T. A. Cain, M. L. C. Buffon, C. Polchinski, S. Stemmer, and S. Rajan, Modulation of over $10^{14}cm^{-2}$ electrons in $SrTiO_3/GdTiO_3$ heterostructures, Appl. Phys. Lett. **104**, 182904 (2014).

[45] M. Mochizuki and M. Imada, G-type antiferromagnetism and orbital ordering due to the crystal field from the rare-earth ions induced by the $GdFeO_3$-type distortion in $RTiO_3$ with R = La,Pr,Nd, and Sm, J. Phys. Soc. Japan **73**, 1833 (2004).

[46] H. D. Zhou and J. B. Goodenough, Localized or itinerant TiO_3 electrons in $RTiO_3$ perovskites, J. Phys.: Condens. Matter **17**, 7395 (2005).

[47] A. C. Komarek, H. Roth, M. Cwik, W.-D. Stein, J. Baier, M. Kriener, F. Bourée, T. Lorenz, and M. Braden, Magnetoelastic coupling in $RTiO_3$ (R = La, Nd, Sm, Gd, Y) investigated with diffraction techniques and thermal expansion measurements, Phys. Rev. B **75**, 224402 (2007).

[48] P. Moetakef, J. Y. Zhang, A. Kozhanov, B. Jalan, R. Seshadri, S. J. Allen, and S. Stemmer, Transport in ferromagnetic $GdTiO_3/SrTiO_3$ heterostructures, Appl. Phys. Lett. **98**, 112110 (2011).

[49] P. Moetakef, J. R. Williams, D. G. Ouellette, A. P. Kajdos, D. Goldhaber-Gordon, S. J. Allen, and S. Stemmer, *Carrier-controlled ferromagnetism in* $SrTiO_3$, Phys. Rev. X **2**, 021014 (2012).

[50] C. A. Jackson and S. Stemmer, Interface-induced magnetism in perovskite quantum wells, Phys. Rev. B **88**, 180403 (2013).

[51] J. Y. Zhang, C. A. Jackson, S. Raghavan, J. Hwang, and S. Stemmer, Magnetism and local structure in low-dimensional Mott insulating $GdTiO_3$, Phys. Rev. B **88**, 121104 (2013).

[52] S. Raghavan, S. J. Allen, and S. Stemmer, Subband structure of two-dimensional electron gases in $SrTiO_3$, Appl. Phys. Lett. **103**, 212103 (2014).

[53] A. Janotti, L. Bjaalie, B. Himmetoglu, and C. G. Van de Walle, Band alignment at band-insulator/Mott-insulator interfaces, Phys. Status Solidi RRL **8**, 577 (2014).

[54] L. Bjaalie, B. Himmetoglu, L. Weston, A. Janotti, and C. G. Van de Walle, Oxide interfaces for novel electronic applications, New J. Phys. **16**, 025005 (2014).

[55] R. Chen, S. Lee, and L. Balents, Dimer Mott insulator in an oxide heterostructure, Phys. Rev. B **87**, 161119 (2013).

[56] L. Bjaalie, A. Janotti, B. Himmetoglu, and C. G. Van de Walle. Turning $SrTiO_3$ into a Mott insulator, Phys. Rev. B **90**, 195117 (2014).

[57] A. Janotti, L. Bjaalie, L. Gordon, and C. G. Van de Walle. Controlling the density of the two-dimensional electron gas at the $SrTiO_3/LaAlO_3$ interface, Phys. Rev. B **86**, 241108(R) (2012).

[58] H. Banerjee, S. Banerjee, M. Randeria, and T. Saha-Dasgupta, Electronic structure of oxide interfaces: A comparative analysis of $GdTiO_3/SrTiO_3$ and $LaAlO_3/SrTiO_3$ interfaces, Sci. Rep. **5**, 18647 (2015).

[59] G. Kresse and J. Furthmüller, Efficient iterative schemes for *ab initio* total-energy calculations using a plane-wave basis set, Phys. Rev. B **54**, 11169 (1996).

[60] J. Perdew, K. Burke, and M. Ernzerhof, Generalized Gradient Approximation Made Simple, Phys. Rev. Lett. **77**, 3865 (1996).

[61] V. I. Anisimov, F Aryasetiawanz, and A. I. Lichtenstein, First-principles calculations of the electronic structure and spectra of strongly correlated systems: The LDA + U method, J. Phys.: Cond. Mat. **9**, 767 (1997).

[62] See Supplemental Material at http://link.aps.org/supplemental/10.1103/PhysRevB.96.045113 for band structures of $RTiO_3$ bulk and $RTiO_3/SrTiO_3$(R = La,Gd) heterostructures.

[63] B. Yin, P. Aguado-Puente, S. Qu, and E. Artacho, Two-dimensional electron gas at the $PbTiO_3/SrTiO_3$ interface: An *ab initio* study, Phys. Rev. B **92**, 115406 (2015).

[64] A. P. Petrovic, A. Pare, T. R. Paudel, K. Lee, S. Holmes, C. H. W. Barnes, A. David, T. Wu, E. Y. Tsymbal, and C. Panagopoulos, Long-range electronic reconstruction to a $d_{xz,yz}$-dominated Fermi surface below the $LaAlO_3/SrTiO_3$ interface, Sci. Rep. **4**, 5338 (2014).